CrystEngComm

Directed synthesis of aragonite through semi-continuous seeded crystallization methods for CO2 utilization

Journal:	*CrystEngComm*
Manuscript ID	CE-ART-08-2023-000809.R1
Article Type:	Paper
Date Submitted by the Author:	02-Oct-2023

Complete List of Authors:	Williams, Jonah ; Columbia University, Earth and Environmental Engineering Zhao, Diandian; Columbia University, Department of Civil Engineering and Engineering Mechanics; Columbia University, Lenfest Center for Sustainable Energy Zhang, Ning; Columbia University, Earth and Environmental Engineering; Columbia University, Lenfest Center for Sustainable Energy Chin, Aysha; Rochester Institute of Technology, Chemical Engineering Kawashima, Shiho; Columbia University, Civil Engineering and Engineering Mechanics Moment, Aaron; Columbia University, Chemical Engineering

Title:
Directed synthesis of aragonite through semi-continuous seeded crystallization methods for CO_2 utilization

Authors:
Jonah M. Williams[1,2], Diandian Zhao[2,3], Ning Zhang[1,2], Aysha Chin[4], Shiho Kawashima[2,3], and Aaron J. Moment[2,5,§]

[1]Department of Earth and Environmental Engineering, Columbia University, New York, New York, 10027
[2]Lenfest Center for Sustainable Energy, Columbia University, New York, New York, 10027
[3]Department of Civil Engineering and Engineering Mechanics, Columbia University, New York, New York, 10027
[4]Department of Chemical Engineering, Rochester Institute of Technology, Rochester, New York, 14623
[5]Department of Chemical Engineering, Columbia University, New York, New York, 10027

§**Author to whom correspondence should be issued:** Aaron Moment, Professor of Professional Practice in Department of Chemical Engineering, 803 S.W. Mudd Hall, Mail Code 4721, 500 W 120th Street, New York, New York 10027. Email: ajm2293@columbia.edu, Tel.: (212)-853-1829

Keywords: aragonite, precipitated calcium carbonate, carbon capture utilization and storage, semi-continuous crystallization, crystal seeding, polymorphism

Abbreviations: PCC, precipitated calcium carbonate; CCUS, carbon capture utilization and storage; OPC, ordinary Portland Cement; HCP, hydrated cement paste; C&DW, construction and demolition waste; CDR, carbon dioxide removal; ACC, amorphous calcium carbonate

Draft Date: 09/29/2023

Abstract:
The synthesis of high-purity precipitated calcium carbonate (PCC) is responsible for approximately 30% of the global annual production of calcium carbonates. As increasing carbon capture utilization and storage (CCUS) facilities come online to mitigate anthropogenic emissions, PCC production is expected to grow through carbon mineralization production pathways. Tuning the PCC morphological and crystal structure properties will largely dictate the potential downstream uses of the carbonate products; thus, increased research is needed into process design considerations for crystal habit modification of PCC. Of the three anhydrous polymorphic forms of PCC, aragonite shows great promise in applications as a filler material or flow-modifier due to its unique needle-like structure. Synthetic aragonite is generally produced at elevated reaction temperatures (60-80^{o}C), however alternative crystallization methods can be applied to reduce this energy barrier and better control crystal production. Herein, we compare the crystallization of aragonite in both a batch and semi-continuous crystallizers using a model system (e.g., $CaCl_2$ and K_2CO_3) to elucidate the effect of mixing and saturation in relation to PCC crystal morphology. Seeding of aragonite is also utilized as a method to better control the PCC production process and lower the required synthesis temperature to 25-40^{o}C. Finally, these methods are extended to a Ca-rich leachate from waste hydrated cement paste (HCP) for comparison with the model system. The produced aragonite is reincorporated into new cement and tested for its potential hydration and rheological advantages. Overall, this work motivates the use of alternative crystallization methods to promote polymorph control for niche CCUS applications, especially cement decarbonization.

1. Introduction

1.1. Polymorphs of $CaCO_3$ to support carbon capture utilization and storage (CCUS)

Carbon capture utilization and storage (CCUS) encompasses a suite of technologies and processes which aim to recover and dispose of atmospheric or point-source CO_2 linked to anthropogenic climate change.[1–3] Among these routes, carbon mineralization is an attractive method to sequester CO_2 as thermodynamically stable carbonate salts (e.g., $MgCO_3$, $CaCO_3$) which allows for permanent storage of the carbon.[4–6] *Ex-situ* carbon mineralization is anticipated to provide a medium for carbon capture due to the abundance of alkaline industrial wastes.[7,8] These waste include Ca/Mg rich materials, such as mine tailings, construction and demolition waste (C&DW), steel slags, desalination brines, etc.[9,10] The end use and market value of the carbonates will be largely determined by their purities and associated properties, especially their crystal structure and morphologies.[6,11] Precipitated calcium carbonate (PCC) is a natural target for the carbon mineralization of Ca-bearing alkaline wastes due to the numerous industrial uses of $CaCO_3$. The three different anhydrous polymorphs of $CaCO_3$, vaterite, aragonite, and calcite (listed in order of thermodynamic stability), can be produced synthetically using high purity model salts (e.g., $CaCl_2$ and K_2CO_3).[12,13] Numerous studies have attempted to elucidate the salient properties involved in the crystallization of each of these polymorphs and their associated crystal structural differences. As shown in **Figure 1.1**, these three polymorphs have distinctly different crystal structures with aragonite being mostly orthorhombic, calcite being rhomboedric, and vaterite being mostly hexagonal.[12,14] These structural differences are reflected in the individual crystal habits and allow for potential niche applications of the uncommon metastable PCC polymorphs, aragonite and vaterite.[11,12] Tuning *ex-situ* carbon mineralization reactions to produce these three distinct PCC polymorphs with potential market value gives CCUS increased motivation.

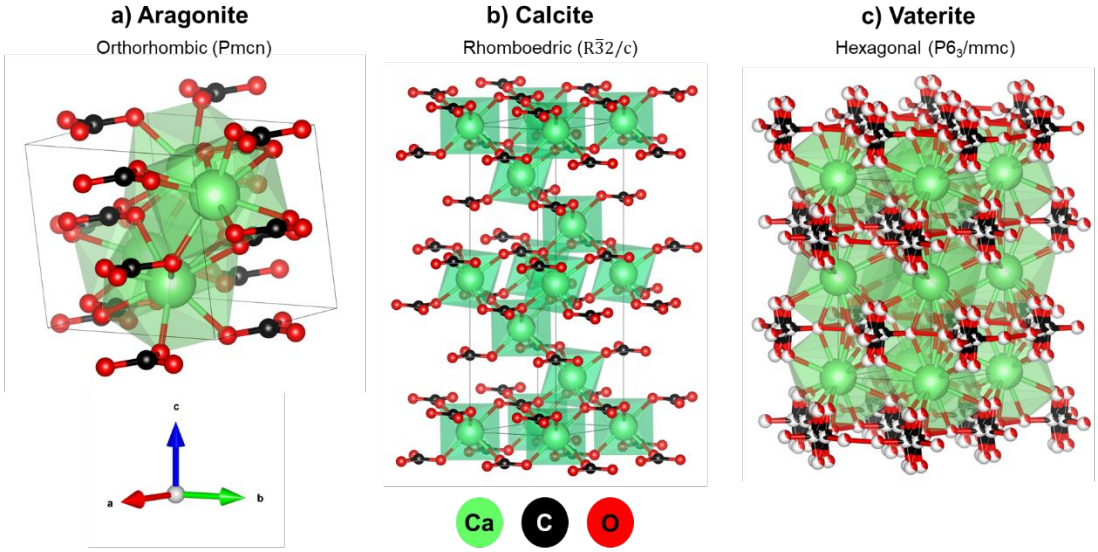

Figure 1.1. Crystal structure visualization of the three anhydrous polymorphs of $CaCO_3$ which includes **(a)** aragonite, which can be orthorhombic, **(b)** calcite, which can be rhomboedric and **(c)** vaterite, which can be hexagonal. Structures obtained from the Cambridge Crystallographic Data Center (CCDC) and plotted in VESTA.

1.2. Properties of aragonite and its advantages

Of the three anhydrous PCC polymorphs, aragonite stands out due to its characteristic "needle-like" crystal habit. This generally gives synthetic aragonite a lower median particle size (D_{50}), a higher relative surface area, and higher aspect ratio (length-to-width) crystals when compared to vaterite and calcite prepared in a similar manner.[11,12] **Figure 1.2** provides an overview of the bulk properties, natural occurrences, and industrial uses of aragonite. Within the natural environment, aragonite can be found in high pressure

metamorphic rock formations, particularly those from subduction areas.[15] It is also found in altered ultramafic systems (e.g., serpentinization) and as a product of carbonic fluid-rock interactions in the hadal zone.[15] Aragonite is a major component of bivalve, mollusk, and certain coral shells/exoskeletons.[13,16] It is theorized that these organisms form aragonite, even in calcite saturated waters, by using special enzymes and proteins in a biomineralization process(es).[17] As such, it can also be found as a component of oolite sedimentary rocks, the remnants of some of these same organisms.[18] Aragonite is a metastable polymorph of calcium carbonate, and can transform to calcite if the proper thermodynamic conditions are provided. Previous studies have shown that at high enough temperatures, the crystal structure of aragonite can rearrange to form calcite.[19] In the ocean, one of the largest carbonate sinks, aragonite has a higher solubility than calcite due to its metastability.[20] Aragonite can precipitate even in calcite rich waters, generally due to localized higher Mg>Ca concentrations; a ratio of 2:1 Mg:Ca has been shown as the threshold for aragonite precipitation in the ocean.[20,21]

The unique shape of aragonite is theorized to impart properties which are advantageous for certain industrial applications. For instance, Kohler et al. (2007) reported on the biogenic removal of metal ions such as cadmium, lead, and zinc using aragonite derived from marine species.[22] Aragonite is an attractive filler for rubbers, polymers, paints, and plastics and Thenepalli et al. (2015) suggest that aragonite can be a useful filler for polypropylene materials.[23] It is commonly used in paper making as a material to increase whiteness while enhancing the printability of paper. Hu et al. (2012) concluded that paper costs can be reduced while using aragonite fillers without sacrificing strength.[24] Aragonite is also used in the manufacture of lime and as a potential filler and additive in cementitious systems, although increased research in this area is warranted. Shen et al. (2022) enumerated the advantages of aragonite whiskers in CO_2-cured concrete as a micro-fiber reinforcement.[25] More recently, Zhao et al. (2023a) showcased the potential advantages of aragonite during the hydration and curing of cement pastes.[26] Additional, Zhao et al. (2023b) also studied the modification of the rheological properties of aragonite-cement paste and its potential use is 3-D concrete printing applications.[27]

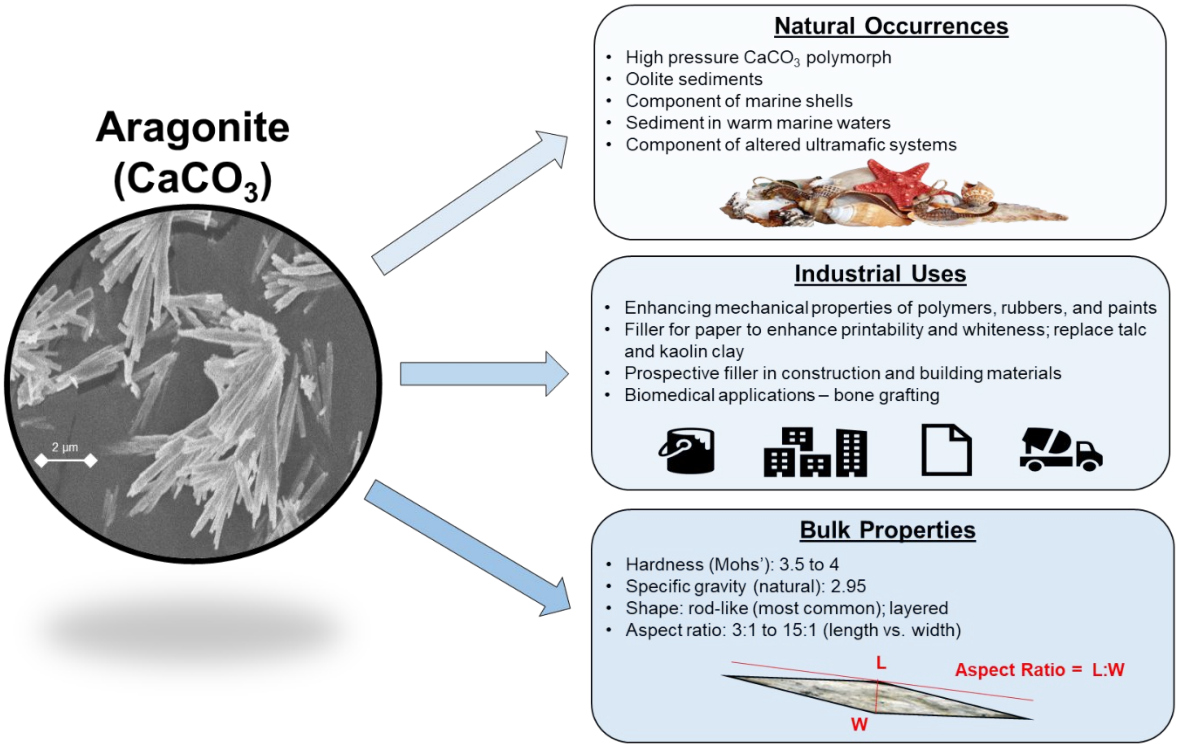

Figure 1.2. The PCC polymorph aragonite, and salient properties such as its natural occurrences, its current and prospective industrial uses, and important bulk properties.

1.3. Synthetic methods to produce high-purity aragonite PCC

Although aragonite is abundant in the crust, sedimentary deposits, and oceans, it is not easily accessible to be industrially utilized. The synthetic production of tunable PCC in the form of aragonite is an attractive and promising pathway to increase the potential uses of carbonates within various industrial supply chains.[6] It can also facilitate and give motivation to CCUS activities if the calcium precursors for the $CaCO_3$ are derived from alkaline wastes and the CO_2 is sourced from carbon dioxide removal (CDR) sites. According to Rim et al. (2021), the CO_2 storage/utilization potential of construction and demolitions waste is high, as roughly 10,300 Mt/year of C&DW is generated.[10] Numerous studies have attempted to describe the ideal conditions for synthetic aragonite production from precursor salts such as calcium chloride or acetate and sodium carbonate, sodium bicarbonate, and ammonium carbonate. Aragonite is considered a more stable thermodynamic phase at higher temperatures in aqueous media, forming an enantiotropic system with calcite; [11,28,29] generally, temperatures above 60°C in the bulk are necessary to see appreciable amounts of aragonite. The kinetics of nucleation and growth of the carbonate phases are also temperature dependent[11], leading to a rich landscape of phase behavior impacted by both kinetic and thermodynamic considerations.[30] Additional studies have used gaseous CO_2 as a carbon source and studied aragonite production from $Ca(OH)_2$ slurries and supersaturated solutions of $CaCl_2$; however, as Liendo et al. (2022) points out these systems often suffer from slow precipitation kinetics due to mass transfer limitations by both CO_2 diffusion and $Ca(OH)_2$ solubility.[31] Other researchers have attempted to isolate aragonite via inducing the transformation of vaterite to aragonite, which has been shown by Cherkas et al. (2018) using deionized water at high temperatures and by Konopacka-Lyskawa et al. (2020) suing solvent mixtures of DMSO/EtOH.[32,33] Walker et al. (2017) documented a purely solid-state transition from amorphous calcium carbonate (ACC) directly to aragonite using CryoTEM.[34] Novel approaches, such as confined space aragonite crystallization in micropores without any additives can also suppress calcite formation.[35,36] Reimagined reactor systems, such as continuous gas-liquid tubular reactors have also been shown to produce aragonite using additives such as Mg^{2+} ions in the presence of Ni-nanoparticles.[37] A significant amount of research has been conducted in the area of $CaCO_3$ nucleation, precipitation, and morphological tuning; however, there is an absence of studies aimed at integrating these systems with CCUS technologies utilizing unique production approaches. Additionally, for the metastable phase of aragonite, increased studies toward realizing the potential uses for this unique polymorph are needed.

1.4. Semi-continuous seeded crystallization as a potential method for aragonite synthesis

Crystal seeding has been well studied as a method to reduce the energy barrier for nucleation of certain polymorphs at various conditions.[38,39] Industrially, it is commonly used as a method to preferentially form high-value molecules such as pharmaceuticals and medical compounds. It has previously been applied to $MgCO_3$ to produce magnesite as opposed to hydromagnesite at lower temperatures.[40] Crystal seeding has also been applied to PCC production in an attempt to isolate specific crystal habits and polymorphs and as a nucleation enhancement; however, only a few studies have targeted aragonite, specifically. Berner (1975) published an early study showcasing the effect of Mg^{2+} on poisoning calcite growth from seed crystals, while the presence of Mg^{2+} enhanced the growth of aragonite from seeds.[41] Seeding has also been used to selectively precipitate aragonite PCC from seawater treatment facilitates to avoid calcite fouling downstream[42] and in the cooling of water from geothermal sinks.[43] Porous aragonite was synthesized in the presence of silicates using aragonite seeds[44] and through a CO_2-bubbling system using $Ca(OH)_2$-$MgCl_2$ as a precursor.[45] Interestingly, Tadier et al. (2016) show that crystallization of aragonite on seeds seems to be a surface-linked diffusive phenomenon and the presence of orthophosphate can inhibit aragonite synthesis.[46]

Different crystallizer designs can also impact performance, yield, and morphology of the precipitates.[47,48] Semi-continuous crystallizers are attractive because they allow for easy integration of seed beds and enhanced nucleation through draw-offs and recycle injection loops, especially in comparison to

batch systems which are conventionally used for high-purity seeded crystallizations.[49] Additionally, these systems can be adapted towards continuous designs by running them slightly out of equilibrium and staging them. In this study, we examine the use of crystal seeding to control the nucleation and synthesis of aragonite in both batch and semi-continuous crystallization reactors. High purity PCC polymorph (vaterite, aragonite, calcite) crystal seeds are synthesized from precursor salts and characterized. Calcium from a soluble salt (i.e., $CaCl_2$) and calcium from the leachate of waste hydrated cement paste (HCP) are utilized during seeded crystallization of aragonite in both batch and semi-continuous reactors. Waste HCP was leached using HCl to recover a Ca-rich liquor for use during carbonation, along with associated Si, Fe, and Al, the other major constituents of cement paste. The comparison between a model Ca-salt (i.e., $CaCl_2$) and the waste HCP was performed to assess the degree to which aragonite production could be controlled in a system which mimics a true carbon mineralization from alkaline waste process. Crystallization temperature, seed loading, and differences in the hydrodynamics of batch and semi-continuous are analyzed for their effect on aragonite yield and properties. Finally, the produced aragonite is re-incorporated into new cement mixtures and its reactivity and rheological properties as an upcycled cement filler are tested. Due to its shape and size, aragonite is posited to be advantageous as a structural filling material and flow modifier compared to conventional calcite or limestone. The replacement of OPC with aragonite fillers in the creation of new cement could offer an additional avenue for the decarbonization of the built environment while imparting advantageous structural properties on the cement itself.

2. Materials and methods

2.1. Materials

The calcium source use to prepare the crystal seeds and for the model salt reactions was $CaCl_2$ (>93%, Sigma-Aldrich Chemicals, USA) prepared at 0.2 M stock solutions. The calcium source from the alkaline waste system was obtained from leached ordinary Portland cement (OPC) which had been hydrated and cured for 1 year with a calcium content of approximately 60 wt.%. HCl (37% ThermoFischer, USA) was used for leaching and NaOH (25% v/v, ThermoFischer, USA) was used to increase the pH of the reaction liquor after leaching. The carbonate source used throughout was K_2CO_3 (99%, anhydrous, Alfa Aesar. ThermoFischer, USA), selected for its high solubility, which was prepared at 0.1 M stock solutions. As a proof-of-concept, KOH (100%, Sigma-Aldrich Chemicals) was loaded with CO_2 gas (100% bone-dry, Airgas, Air Liquide, PA, USA) in deionized water to produce K_2CO_3. This experiment was performed to assess the CO_2-loading capacity of KOH in an aqueous solution which would be reflective of a potential alkaline-slurry CCUS process.[50]

2.2. Methods

2.2.1. Leaching of pH-swing of Ca-rich construction and demolition waste (C&DW)

The leaching of the HCP was performed in a 500 mL ChemGlass (Vineland, NJ, USA) reactor with temperature control to 25^{o}C using a water bath. 300 mL of deionized water was charged into the reactor, and the pH was adjusted to 3 with HCl. 15 grams of HCP sieved to a particle size range between 150-210 µm was added to the reactor at 900 rpm and allowed to react for 60 minutes. This was done to achieve a slurry density (or solid-to-liquid ratio) of 5%. HCl was continually dosed into the reactor to maintain the pH consistently at 3 to ensure adequate leaching was achieved. Afterwards, the reaction liquor was filtered using a Buchner apparatus and the leachate was separated from the unreacted residue. The leachate was returned to the reactor and the pH was increased from 3 to 9 using ("pH-swing process") NaOH in an attempt to remove the ancillary ions of Si, Al, and Fe which are also extracted during the leaching of the HCP.[29] **Figure S1a** shows the leaching kinetics as measured by ICP-OES of the HCP over 60 minutes, yielding a 60% Ca extraction efficiency in a single batch-reactor pass. **Figure S1b** shows the pH-swing process and the concentration of Ca, Si, Al, and Fe as a function of pH. The leachate was diluted with water to bring the Ca^{2+} concentration from 0.32 M to 0.2 M before crystallization as a comparison to the model salt Ca^{2+} stock.

2.2.2. Loading of KOH with CO_2 to produce K_2CO_3

As a proof-of-concept, potassium hydroxide (99%, Sigma-Aldrich Chemicals, USA) was carbonated for 8-minutes at a 0.2M concentration in aqueous media with bubbling CO_2 injected through a ceramic sparger. The stirring rate of the reactor was 600 rpm and the temperature was controlled to 25°C. The reaction was stopped when the pH decrease began to level off around 10 (**Fig. S2a**). After carbonation, the water was evaporated from the sample and the produced K_2CO_3 was characterized and confirmed to be carbonate based on FTIR analysis (**Fig. S2b**) with a yield of 97% and CO_2-capture efficiency of 86% (**Fig. S2d**).

2.2.3. Batch and semi-continuous crystallization

The crystallization reactions were performed in a 500 mL ChemGlass (Vineland, NJ, USA) reaction vessel equipped with temperature control and overhead agitation at 600 rpm. In each crystallization case, 0.1 M K_2CO_3 was charged into the reactor (100mL) and 0.2 M $CaCl_2$ or the leachate of the waste HCP was injected into the reactor via a syringe pump (50 mL). In most cases the injection rate was about 6.7 mL/min, unless otherwise noted. After injection, the crystallization liquor was allowed to age for 23 minutes prior to filtration, EtOH washing, and drying. **Figure 2.1** showcases the process differences between the batch and semi-continuous operating modes. In the semi-continuous mode, the Ca^{2+} was injected into a 120° glass tee on a K_2CO_3-$CaCO_3$ recirculation loop that was circulated via peristaltic MasterFlex pump at an average flow rate of 4 mL/s through 1/16" PTFE tubing. After injection and mixing with the circulating liquid, the reaction liquor is routed through the tube-side of a temperature-controlled Graham condenser before returning to the ChemGlass reaction vessel (**Fig. S3**). The MasterFlex recirculation pump was calibrated as a function of mass/volume flow in an effort to assess mass transfer properties of the system (**Fig S4a**) and the residence time was determined as a function of flowrate using dye-tracer testing (**Fig S4b**). In the case where crystal seeds were utilized, they were charged into the circulating tank of either reactor and allowed to disperse into the K_2CO_3 solution prior to injection of the calcium solution. Crystal seed load is defined in terms of slurry density, or solid-to-liquid ratio. This is given as the aragonite seed load in mass versus the total crystallization volume. For instance, at a 1 wt.% S/L aragonite seed load, approximately 1.5 grams of aragonite seed is loaded into a final volume of 150 mL. In the cases where leached HCP was used as the Ca^{2+} source, two main cases were tested using the leachate solution at pH 3 containing Ca, Al, Fe, and Si, and using the solution at pH 9 after a pH-swing containing mostly pure Ca.

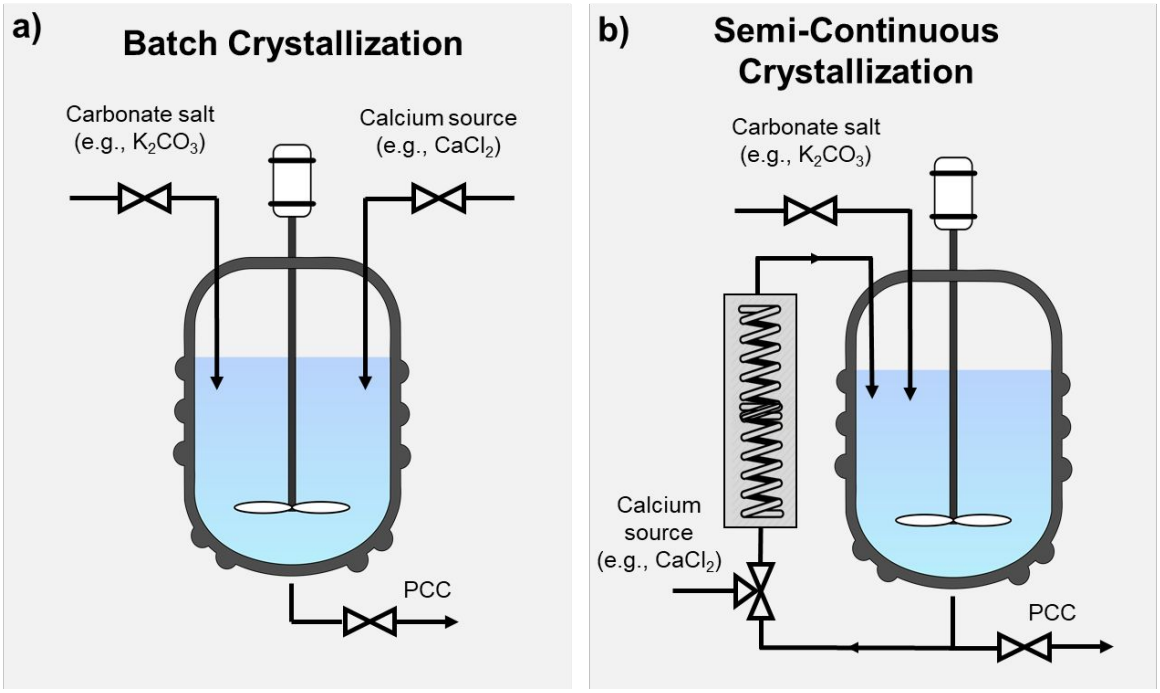

Figure 2.1. (a) Experimental set-up showing the batch crystallizer which includes injection ports and overhead mixing. **(b)** Experimental set-up showing the semi-continuous crystallizer with the recirculation loop passing through both the 120° calcium injection tee and the Graham condenser mixing coil.

2.2.4. Preparation of PCC polymorph crystal seeds

PCC polymorphs vaterite, aragonite, and calcite were synthesized using conventional batch crystallization techniques that were scaled up to obtain sufficient samples (200 g) for seeding applications. Crystallization experiments of four liters were designed to yield approximately 200 grams of PCC in a single batch. The precursor salts for each are $CaCl_2$ and K_2CO_3 as described in **Section 2.1**. To isolate calcite and aragonite, 221 grams of $CaCl_2$ and 276 grams of K_2CO_3 were dissolved separately in two 4-liter beakers of deionized water. For calcite synthesis, the calcium solution was slowly added to the potassium solution and the mixture was aged and thoroughly mixed for 16 hours at 600 RPM. In the case of aragonite production, the stock solutions were heated to approximately 80 ºC before mixing, and the solutions were aged for 30 minutes before undergoing filtration and drying. During this time the temperature of the vessel was controlled via a temperature-controlled hotplate. To isolate the least stable form of PCC, vaterite, 106 grams of NH_4Cl (99%, Sigma-Aldrich Chemicals, USA) was added to the calcium solution before crystallization. Additionally, the carbonate amount was doubled (552 g) to increase the ionic strength of the solution as reported by reference studies which successfully made vaterite.[19,33,51,52] The solutions were mixed, aged for only 10 minutes, and then rapidly filtered and rinsed with ethanol to prevent vaterite transformation. All PCC samples were filtered using a Buchner vacuum apparatus, rinsed with 80% ethanol, and subsequently dried overnight at 80 ºC in a vacuum oven.

2.2.5. Characterization and analytical techniques

2.2.5.1. Powder X-ray diffractometry (PXRD)

Powder X-ray diffraction (PXRD) was employed to analyze the powdered carbonate samples following crystallization. Phase identification was carried out using the Bragg-Brentano geometry, and phase quantification was achieved through Rietveld refinement. The analysis utilized a Panalytical X'pert3 Powder XRD instrument (Malvern Panalytical) equipped with a 3 kW Cu long line focus X-ray generator

and a PIXcel 1d detector. To refine the spectral data and calculate the mass percentage for each polymorphic phase present, open-source material analysis using diffraction (MAUD) software was employed. Reference spectral data for fitting the carbonate mixtures were obtained from the Inorganic Crystal Structure Database (ICSD) with the following identification numbers: vaterite (15879), calcite (73446), and aragonite (170225). This was the major technique employed to provide quantitative compositional data on the crystalline phases present throughout each experiment. When crystal seeding experiments were conducted, the reported mass balance of the crystalline phase reflects the subtraction of the seed crystals from the mass balance in an effort to accurately depict the newly created mass.

2.2.5.2. Scanning electron microscopy with energy-dispersive x-ray spectroscopy (SEM-EDS)

The morphologies of the $CaCO_3$ crystals was studied via SEM using a a Zeiss SIGMA VP with 12 angstrom resolution and acceleration voltages of 10 kV. PCC samples were sputter coated with a 1 nm layer of AuPd prior to imaging. Elemental analysis was performed using energy-dispersive x-ray spectroscopy (EDS) with a Bruker XFlash 6-30 detector at a resolution up to 5 nm.

2.2.5.3. Attenuated total reflectance Fourier transform infrared spectroscopy (ATR-FTIR)

Attenuated total reflectance Fourier transform infrared spectroscopy (ATR-FTIR) was used study the morphologies of the produced carbonate crystals. A Nicolet iS50 FTIR Spectrometer (ThermoFisher Scientific) was used to collect FTIR spectral data and automatically subtracted the background data prior to each sample measurement. 64 scans were collected and averaged to produce each spectrum.

2.2.5.4. Coulometric carbon analysis

A UIC Coulometrics (CM150) Carbon Analyzer equipped with a total carbon (TC) furnace module and total inorganic carbon (TIC) acidification module was used to study the purity of the carbonates produced from the Ca-leachate source. The purity of the carbonates was determined by dissolving the sample in 2N perchloric acid and measuring the CO_2-degassed using an electrochemical cell with Pt-cathode in MEA and Ag-anode in DMSO/potassium iodide.

2.2.5.5. Particle size analysis (PSA)

Particle size distributions (PSD) of the produced PCC were monitored using particle size analysis (PSA) via a Beckman-Coulter LS-13-320 laser diffractometer multi-wavelength instrument. The carbonate samples were loaded to reach an optical coverage of approx. 5% and suspended in an aqueous column while measured for 120 second using three different optical filters. The resulting data was averaged to produce the required distributions.

2.2.5.6. Cement paste calorimetry and rheology testing

The produced aragonite was used to prepare cement paste specimens to compare to calcite-OPC and conventional OPC reference samples. Produced aragonite and calcite were used to replace 20 wt.% cement paste in the creation of new admixtures. The dry powders of carbonates and OPC were mixed by hand homogenously before adding water. Then, distilled water was added to a final water-to-solid (w/s) ratio of 0.4, and the paste was mixed for 2 min. ~5 g of paste was loaded into a glass ampule for calorimetric testing. A TAM Air Isothermal Calorimeter was utilized with distilled water as a reference and the heat flow from the samples was monitored for 168 h. For rheological testing, a ThermoScientific HAAKE MARS rheometer was loaded with ~50 g of cement paste specimens and a 220 s^{-1} rotational pre-shear was applied to ensure all samples reached the same reference state. The rheological testing was performed 10 min after the water was added and mixed within the cement paste. During measurement, a constant shear rate of 0.1 s^{-1} was applied to measure both static and dynamic yield stresses.

3. Results and discussion

3.1. Properties and characterization of PCC polymorph seeds

The produced PCC crystal seeds assumed the expected morphologies as shown in **Figure 3.1a.** The presence of calcite, vaterite, and aragonite was detected using FTIR (**Fig. 3.2b**) and the composition of the crystalline phase was up to 99% pure in the calcite and vaterite seeds, with 86% purity being achieved in the aragonite case (**Fig. 3.2c**). The remainder of the aragonite sample was determined to be largely calcite, likely an artifact of the scaled-up production process described in **Section 2.2.3.** Additional properties were also established, such as the BET surface area (**Fig. S5a**) and particle size distributions (**Fig. S5b**) which showcased aragonite having the largest surface area at 8 m^2/g and the smallest medial particle size at 5.2 µm. Aragonite was also determined to have the smallest bulk density of all the three polymorphs at 0.42 g/cm^3 (**Fig. S5c**) which can also be visualized with it taking up more space in a sample bag at roughly the same weight as the other samples (**Fig. S5d**). These characteristics of aragonite make it a unique polymorph of PCC which could have applications requiring high surface area carbonates with low densities and particle size.

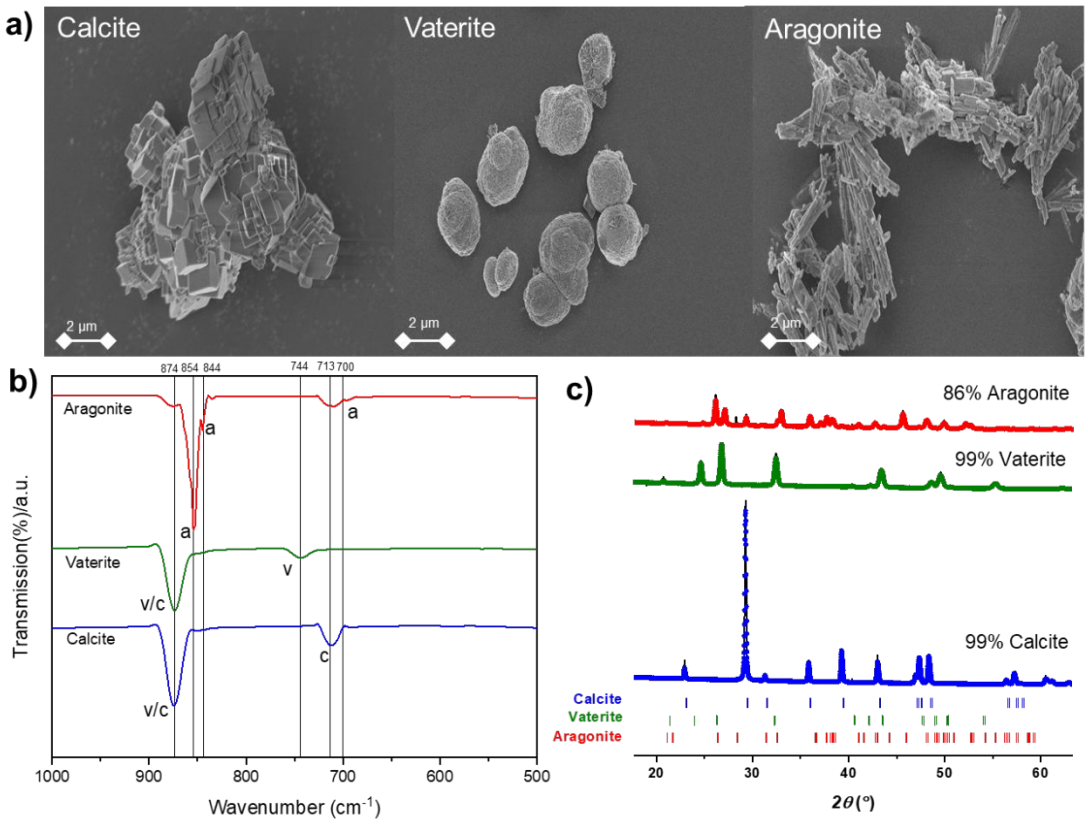

Figure 3.1. (a) SEM images, **(b)** FTIR spectral data, and **(c)** PXRD data of the produced PCC polymorph crystal seeds confirming the existence of each of the three $CaCO_3$ polymorphs, vaterite, aragonite, and calcite. Black lines in the PXRD data indicate the fitted data using Rietveld refinement.

3.2. Semi-continuous crystallization reduces the temperature required to produce synthetic aragonite

The quantitative-PXRD data for the un-seeded production of aragonite at various temperatures using the model salt system is shown in **Figure 3.2a and 3.2b.** Using un-seeded batch operation, 80 wt.% aragonite was synthesized at 60°C which confirms the results of previous researchers working on similar systems. Interestingly, the use of the semi-continuous operation allowed for the production of aragonite at lower temperatures (**Fig. 3.2a**). FTIR analysis notes the appearance and increased prominence of aragonite peaks at 700, 844, and 854 cm^{-1} at lower temperatures in the semi-continuous crystallizer product compared to the

batch case (**Fig. 3.2c, 3.2d**).[53,54] As the temperature increases from 25°C to 80°C in both cases, the v_3 anti-symmetrical CO_3 vibrational peak grows more intense and shifts from 1465 to 1492 cm^{-1}. This can be attributed to the decrease in vaterite and potential amorphous calcium carbonate (ACC) and increase in aragonite as the temperature increases. The morphologies and crystal habits were analyzed via SEM, supporting the observed PXRD data. Vaterite spheres can been seen at lower temperatures, transforming into agglomerated aragonite clusters in the batch operation case (**Fig. S6**). However, in the semi-continuous operation, distinct aragonite needles can be seen as low as 50-60°C (**Fig. S7**). These observed differences point to the enhanced control for aragonite synthesis which is imparted by semi-continuous un-seeded crystallization, likely a result of improved hydrodynamics and heat transfer and suppression of amorphous and vaterite nucleation even at low temperatures. Particle size analysis (PSA) revealed that the D_{50} value remained substantially lower as the temperature increased in semi-continuous mode versus batch (**Fig. 3.3**), confirming the existence of greater aragonite quantities of smaller size and the growing absence of larger vaterite spheres. The observed differences between batch and semi-continuous un-seeded production of aragonite can likely be attributed to a mixing effect imparted by the semi-continuous crystallizer.

The use of the tee-mixer and recirculation loop allows for enhanced nucleation of aragonite and increased dispersion due to circulation. Such a system can reduce supersaturation of alternate phases, which in turn could reduce their relative nucleation rates when compared with aragonite growth. The homogeneity and smaller mixing zone (**Fig. 3.4a)** imparted by the tee-mixer also allows for slower development of K_2CO_3 supersaturation, which could suppress the nucleation of calcite compared to metastable aragonite. Correspondingly, the increased Re number within the semi-continuous circulation loop and decreased tank residence time (**Fig. 3.4b**) impart more favorable hydrodynamics for the nucleation of aragonite with respect to heat transfer in the system. Energy dissipation in the bulk system was estimated to be about 0.008 W/kg, with a calculated tank blend time of 0.897 s (**Fig 3.4b**). The tube blend time for the semi-continuous crystallization case was estimated at 1.87 s, making the mixing times roughly the same order of magnitude.[55] With similar mixing times and the tank flow conditions being turbulent and the recirculating loop flow conditions being laminar, the hydrodynamics of these two crystallization systems are fundamentally different.

The use of semi-continuous and continuous crystallizers to suppress the nucleation of one crystal phase and favor the formation of another has been well studied, especially in areas such as the pharmaceuticals, fine chemicals, and food industries. Previously, Ghiasi et al. (2020) achieved enhanced particle size control formation of different calcite phases using a multi-process crystallization system.[56] Similarly, Ukrainczyk et al. (2007) observed that temperature and supersaturation were the most important parameters in controlling the morphology of the PCC phases present in the carbonation of slaked lime in a semi-continuous process.[57] Clearly, these systems have crystallization advantages over batch processes in reference to PCC morphology control. Additionally, continuous-type crystallization processes allow for much higher throughputs which could be an ideal choice for the scale-up of such systems for CCUS applications.

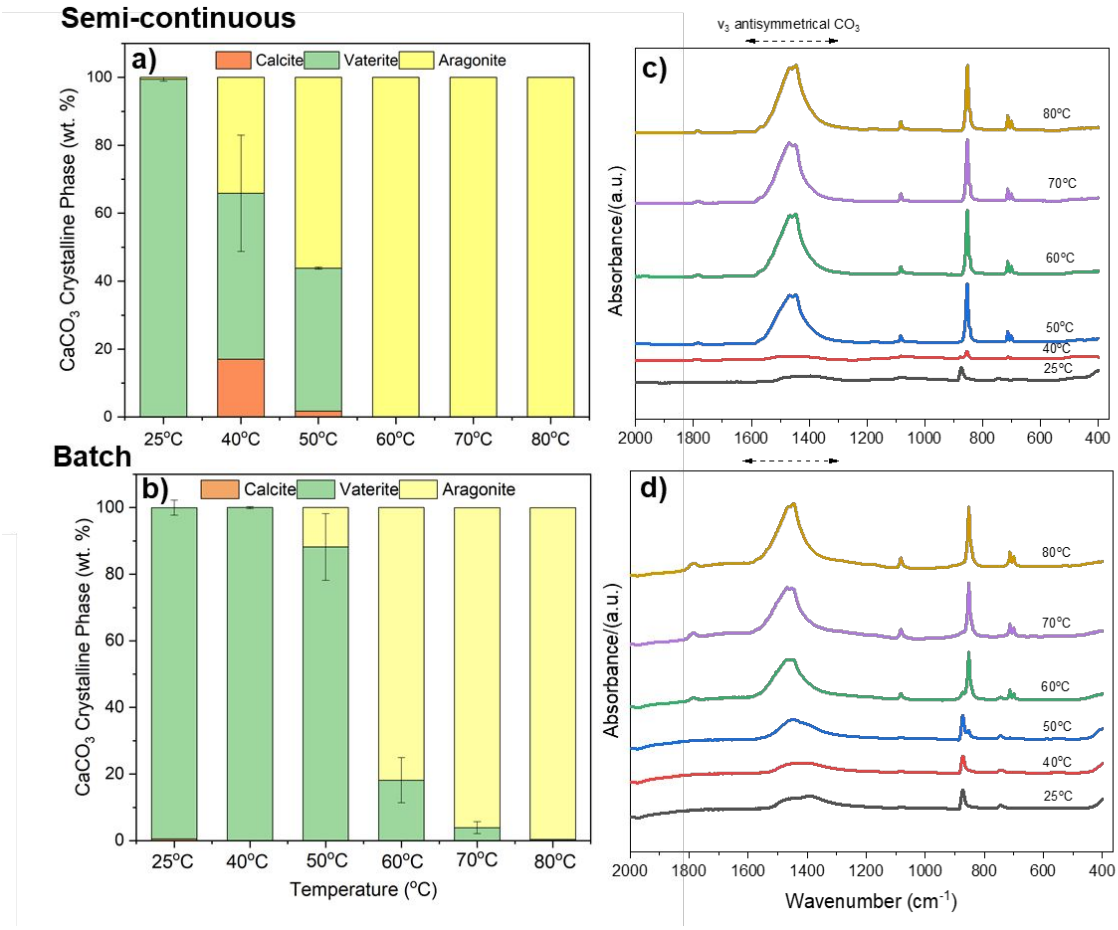

Figure 3.2. Quantitative PXRD data for un-seeded production of PCC in (**a**) semi-continuous and **(b)** batch production methods with associated FTIR spectral data of the produced carbonates in (**c**) semi-continuous and **(d)** batch mode.

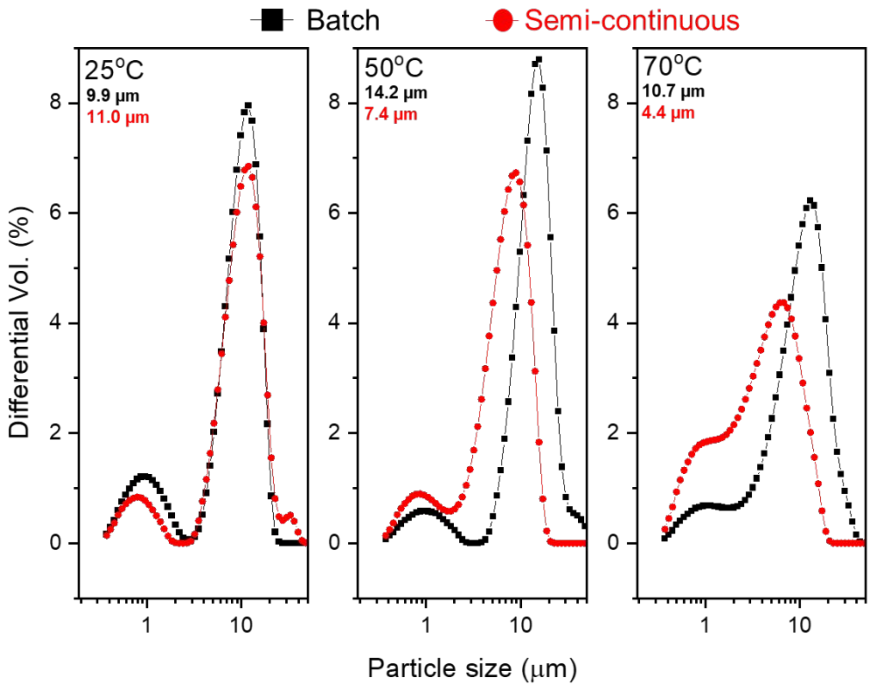

Figure 3.3. Particle size distributions at 25, 50, and 70°C comparing the size control abilities of both batch and semi-continuous unseeded crystallizers for the production of aragonite. Insert particle sizes listed at D_{50} (median) for each case.

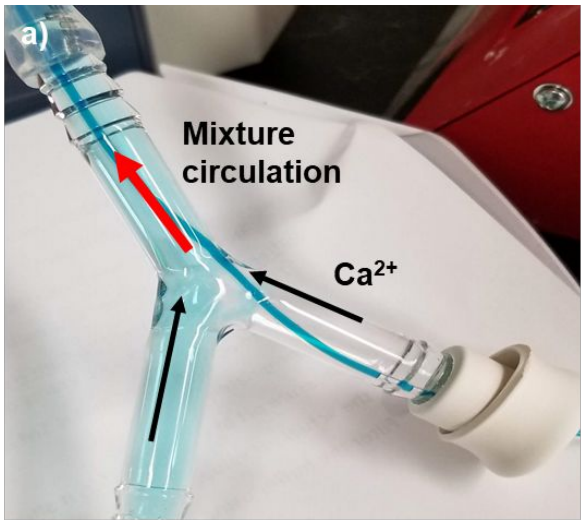

b) Properties	Batch	Semi-Cont.
Avg. Tank Re Number	34675.4	34784.5
Tank Inlet Re Number	105.8	450.0
Impeller Circulation (m^3/s)	0.245	
Syringe Injection Velocity (m/s)	0.147	
Tube Recirculation Velocity (m/s)	N/A	0.068
Energy Dissipation (W/kg)	0.008	
Tank Blend Time (s)	0.897	
Tube Blend Time (s)	N/A	1.87
Velocity Ratio (Inject/Recirc.)	N/A	2.16

Figure 3.4. (a) Image of the mixing tee showcasing the Ca-injection area. **(b)** Table with salient flow properties estimated for each crystallization case.[55]

3.3. Temperature-effect of seeded crystallization processes to make aragonite

Figure 3.5 shows the phase assemblage of the PCC products for both batch and semi-continuous seeded crystallizations as a function of temperature. In this case, 1 wt. % aragonite seed was used, which allowed for a near pure new aragonite product (97-98%) at 60°C. Compared to unseeded production at 60°C, the seeded operation affords a purity increase of approximately 20% when semi-continuous seeded methods were employed. Previous work has shown that 60°C is the temperature at which appreciable amounts of aragonite precipitates in model salt systems; however, that number could be higher if Ca-sources with impurities are used.[12,29] Thus, seeding could prove especially useful to reduce the energetic barrier for

aragonite synthesis, even at lower temperatures through the promotion of heterogenous nucleation.[52,58] Both semi-continuous and batch crystallizers produced similar aragonite phase compositions, with differences mainly relating to the agglomeration and growth of the new aragonite crystals as shown by SEM analysis in **Figure 3.6.** Batch operation resulted in large agglomerated clusters of aragonite, presumably growing on the seed crystals, whereas semi-continuous produced optically less clustered aragonite as the temperature increased. The calculated residence time was almost 23 times lower in the semi-continuous case, likely contributing to the observed particle size results (**Fig 3.4b**). Seeded crystallization methods could be advantageous to produce usable aragonite products at high purity (>86%) at a much lower energy penalty, reducing the overall PCC CO_2-footprint.

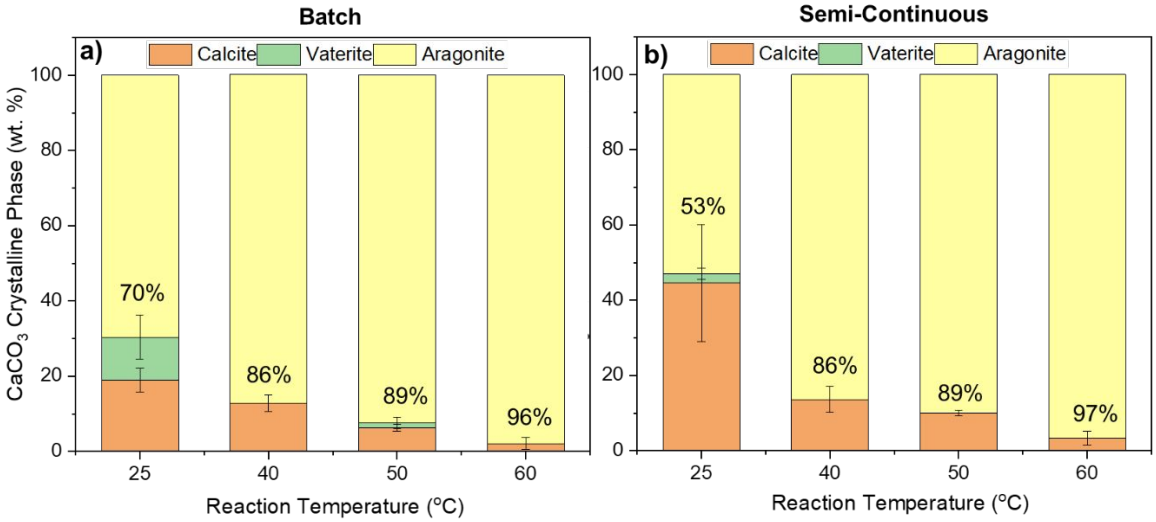

Figure 3.5. (a) Batch and **(b)** semi-continuous crystallization quantitative PXRD data from 25-60°C utilizing 1 wt.% slurry density (solid-to-liquid ratio) aragonite seed bed. Data reflects the subtraction of seed PXRD data from the total yield.

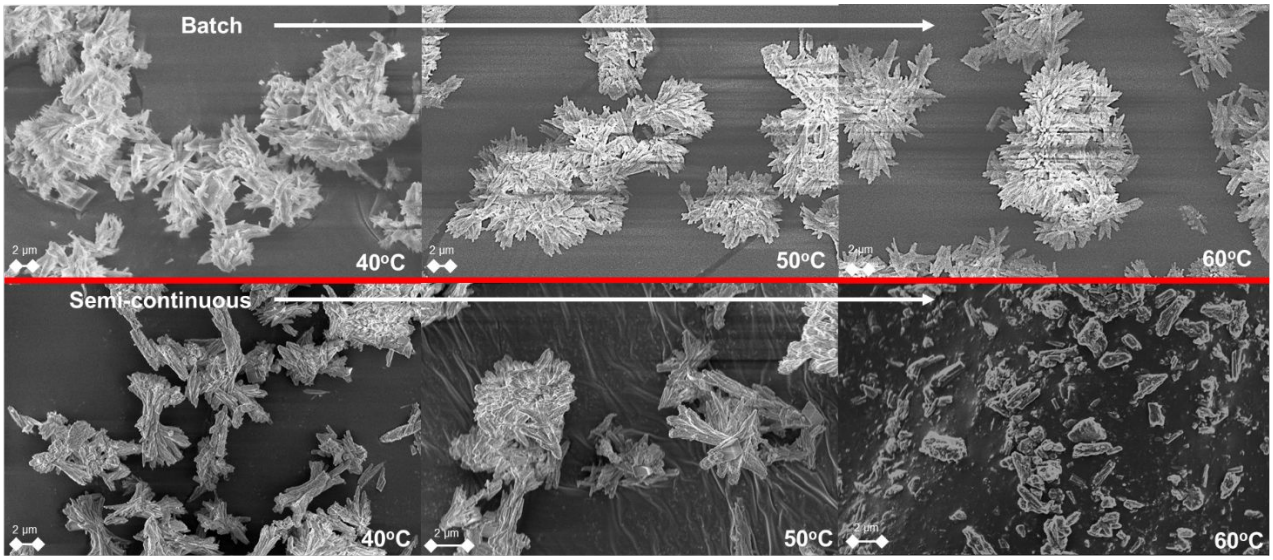

Figure 3.6. SEM images of the batch (top) and semi-continuous (bottom) PCC products at 40, 50, and 60°C at 1wt. % aragonite seed loading.

3.4. Aragonite seed loading at ambient conditions can produce >82% aragonite product

The seed load of aragonite was varied at ambient (25°C) conditions to assess the effect of seed density on the new crystal product. At batch conditions, 78% aragonite was formed at the most extreme seed load of 5 wt.% (**Fig. 3.7a**) whereas the same conditions yielded 82 wt.% aragonite at room temperature using semi-continuous methods (**Fig. 3.7b**); the inability to reach near 100% is likely due to calcite contamination in the starting material. In the batch cases, more vaterite was observed at lower seed densities, which decreased as the seed load increased, which was verified by SEM (**Fig. S9**) and shifts in FTIR peaks from 874 to 854 cm^{-1} (**Fig. S10**). However, using the semi-continuous crystallizer yielded a greater amount of new calcite at seed densities of 0.5-2 wt. % aragonite compared to batch operation. The phenomena could be explained by the enhanced mixing of the semi-continuous system, resulting in lower localized supersaturation and ionic strength which can facilitate the transformation of vaterite to calcite or ACC directly to calcite. Additionally, the presence of some calcite impurities (~14 wt.%) could act as seeds for undesired calcite, especially at low temperatures which disfavor the unseeded synthesis of aragonite. A few studies have reported on the synthesis of aragonite at ambient temperatures; however, additives are generally required such as chelating agents or Mg^{2+}, which can suppress Mg-calcite formation and favor aragonite formation at high supersaturations (>60 mol%) as shown by Park et al. (2008).[59] More complicated techniques can also form aragonite at reduced-temperatures, such as the dry-grinding transformation of calcite to aragonite,[60] confined space suppression of calcite nucleation,[36] and sonication.[61] Directed methods for seeded crystallization could be an advantageous non-additive, ambient system for aragonite production.

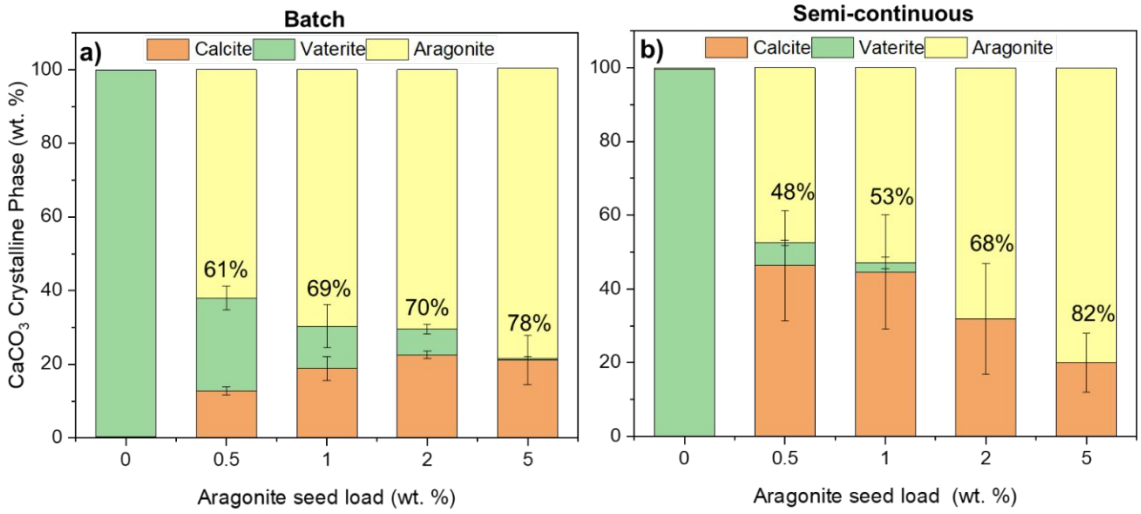

Figure 3.7. (a) Batch and **(b)** semi-continuous crystallization quantitative PXRD data from ambient (25°C) seeding experiment conducted at aragonite seed loads from 0 to 5 wt. %. Data reflects the subtraction of seed PXRD data from the total yield.

3.5. Calcium injection rate has implications for aragonite purity and agglomeration

Figure 3.8 shows the Q-PXRD data for the seeded production of aragonite at room temperature by varying the Ca^{2+} injection rate in batch and semi-continuous operation. Interestingly, the variation of $CaCl_2$ injection rate had little effect on the aragonite quality in batch mode, with purities between 67-7 wt.% being achieved. However, in the semi-continuous crystallizer upwards of 98 wt.% pure aragonite could be formed at 25°C with an inlet rate of 0.83 mL/min. The injection rate also had implications agglomeration, with slower solvent inlet rates leading to more dispersed crystals of a smaller particle size and higher aspect ratio (**Fig. 3.9**). The observed mixing effect imparted by the semi-continuous crystallizer is enhanced as the rate of $CaCl_2$ injection decreases, allowing for controlled nucleation of aragonite on seeds and suppression of calcite co-crystallization. Injection or double-injection crystallizers, where solvent or both solvent/antisolvent are slowly introduced into the vessel have been applied to aragonite synthesis

previously. Ramakrishna et al., (2016) described the production of nano-whisker aragonite at injection rates as low as 0.016 mL/min, whereas Jiang et al. (2009) produced a vaterite/aragonite mixture as low as 40°C using double jet injection of solutions.[62,63] Chen and Xiang (2009) described similar experiments as we report herein, however their double-injection method could not form appreciable aragonite (>60 wt.%) until a temperature of at least 70°C as no seeds were introduced.[64] The use of an aragonite seed bed presents clear advantages with more robust crystallization operations to produce high quality product at ambient conditions.

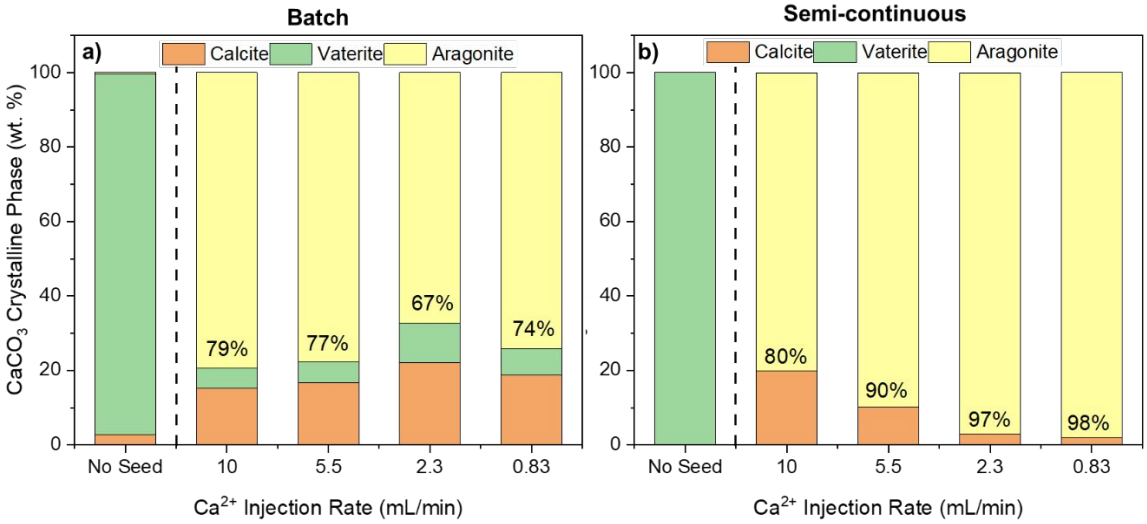

Figure 3.8. (a) Batch and **(b)** semi-continuous crystallization quantitative PXRD data varying the injection rate of Ca from 10 to 0.8 mL/min. Experiments conducted at ambient conditions (25°C) using an aragonite seed load of 1 wt. %.

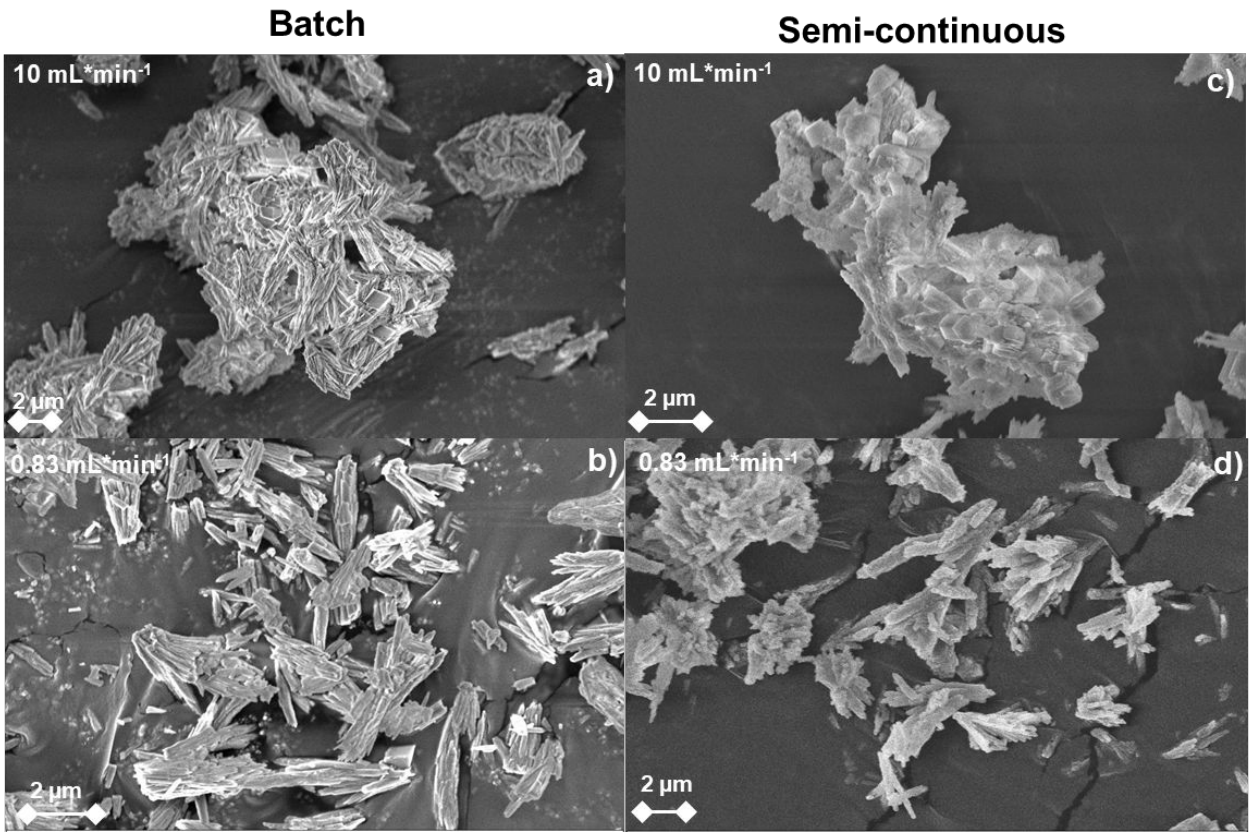

Figure 3.9. SEM images showing the difference between fast Ca injection rate (10 mL/min) and slow Ca injection rate (0.83 mL/min) for both the batch and semi-continuous crystallization operation modes with 1 wt. % aragonite seeding at 25°C.

3.6. Ca-rich leachate from waste hydrated cement paste to produce aragonite

The Ca-rich leachate obtained from the acid digestion of waste hydrated cement paste (**Fig. S1a**) was used as the Ca source to produce PCC in an un-seeded semi-continuous crystallizer. **Figure 3.10** shows the phase assemblage for the PCC products from 25-80°C using pH 3 leachate (no PMO removal) and pH 9 leachate (Si, Fe, Al) removal. It can be observed that the removal of the PMO constituents, Si, Fe, and Al, allow for greater control of the desired metastable phases, with vaterite being prominent below 40°C and aragonite being the main crystalline phase above 40°C. The impurities present in the pH 3 liquid seem to catalyze the formation of calcite, suppression of vaterite, or accelerate the transformation of vaterite to calcite; likely an effect of the increased impurities, such as soluble Si, which may preferentially influence one polymorph over another. Kellermeier et al. (2010) demonstrated the effect of Si on the stabilization of ACC, which overtime directed the precipitation of the ACC to calcite only.[65] Only at 80°C could pure aragonite be formed using the pH 3 liquid. The pH-swing process to remove ions such as Si, Fe, Al, REEs and other precious metals prior to carbonation has been widely studied as a method to concentrate valuable elements from industrials wastes and produce a purer PCC product that can be used downstream.[66,67] The latter is observed in this study, as the PCC produced from pH 3 liquor had a carbonate purity of 67%, whereas the PCC produced from pH 9 liquor reached a purity of 91% as confirmed by carbon analysis and EDS (**Fig. S11a, S11b**); the balance being mainly silica, iron, or aluminum with other trace elements. Similar to our own observations on the production of high-purity carbonates, Zhang and Moment (2023) were able to form vaterite and aragonite from waste concrete leachate, only after it had been purified of Si, Al, and Fe via pH-swing.[29] In order to better control the morphology of PCC and produce metastable phases, vaterite and aragonite, impurities should be removed prior to carbonation.

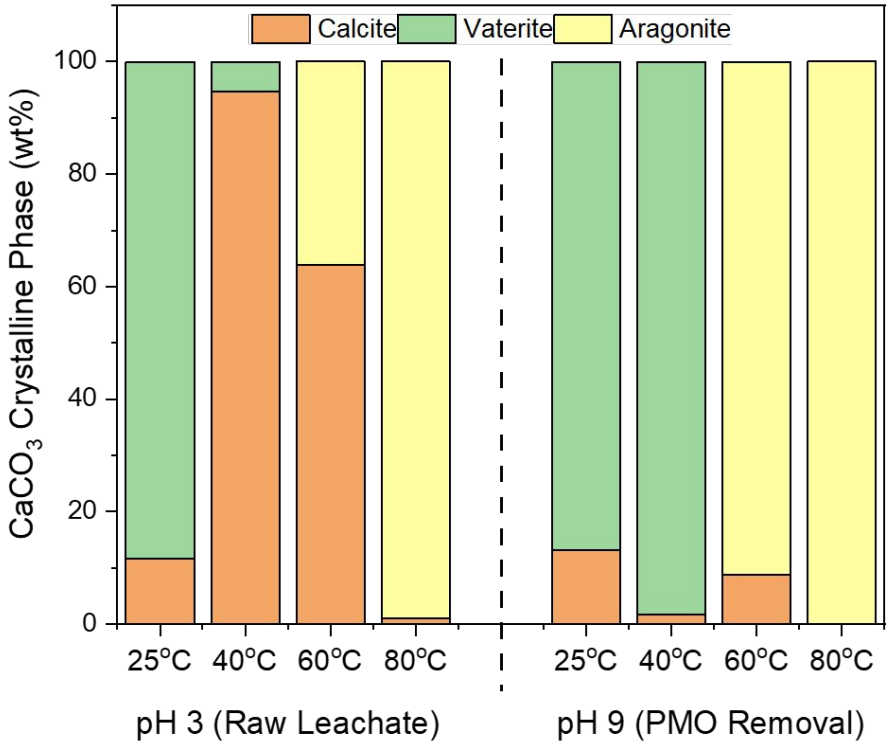

Figure 3.10. Un-seeded semi-continuous PCC production using the Ca-leachate from HCP following direct carbonation at pH 3 and after removing the PMOs at pH 9 from 25 to 80°C.

The use of seeded semi-continuous crystallization using pH 3 and pH 9 leachates was better able to direct the synthesis of aragonite at all conditions studied (**Fig. 3.11)**. The presence of impurities from the use of Ca-rich leachates from alkaline wastes can pose a challenge for crystallization processes, especially when purity and form are highly desired. The use of seeds can be favorable in such systems, as they allow for greater process control when dealing with impurity issues. As seen herein, aragonite seeds afford greater phase purity and form control when utilized. **Figure 3.12a-d** shows the morphologies of the PCC products obtained with and without aragonite seeding at 60°C. At pH 3 unseeded, the presence of calcite and vaterite caked in what appears to the gelation of Si-Fe-Al can be observed. This effect is likely due to the Si-Al-Fe metal oxide residues which can act as a "glue" between particles as the PCC will co-precipitate with the PMOs. The presence of these metal oxides within the carbonates can significantly lower their purity and leads to pure form control. The use of aragonite seeding at pH 3 is useful to promote the nucleation of aragonite even with the presence of these co-ion impurities. Yet, the degree of aragonite agglomeration is quite high, likely a result of the co-precipitation of the Si-Fe-Al oxides and the aragonite itself. After the pH swing process is employed, pH 9, high-purity aragonite can be observed both from a phase wt.% and carbonate purity standpoint. Thus, it appears that seeding with aragonite could be advantageous even in systems where alkaline wastes are used for CCU applications, especially when impurities may be present during carbonation.

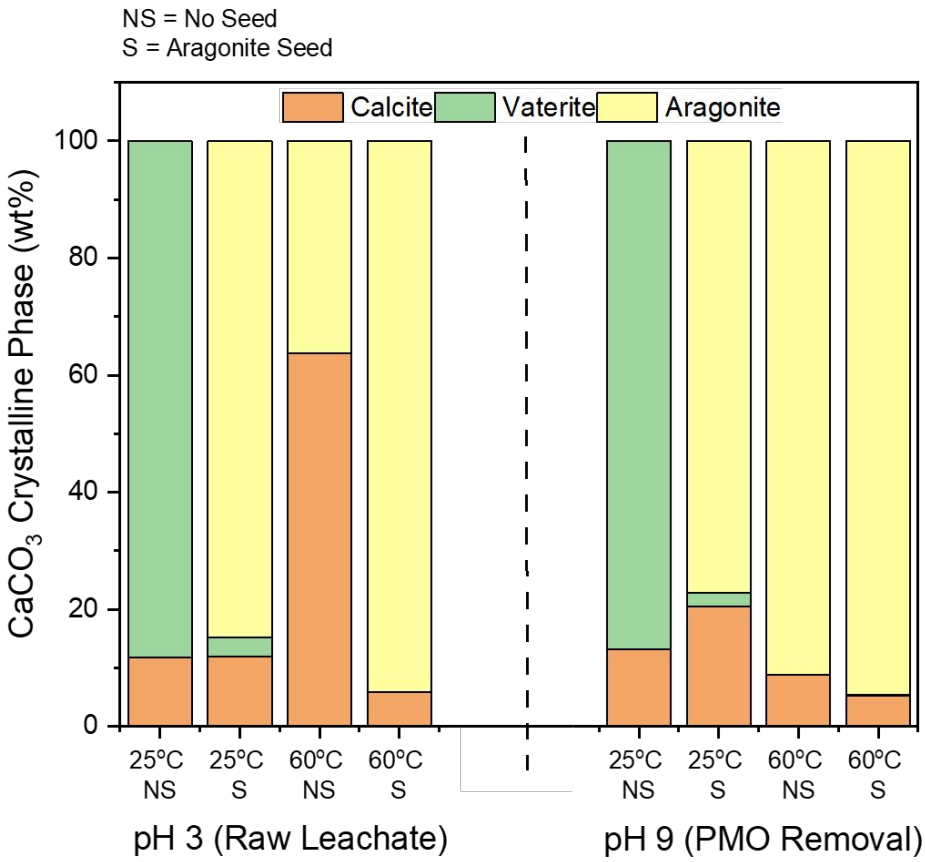

Figure 3.11. Seeded production of aragonite at 25 and 60°C compared to un-seeded production using a semi-continuous crystallization unit operation. Two conditions were tested, one with the Ca-leachate at pH 3 (no pH-swing; Al, Fe, Si present) and another at pH 9 (after pH-swing, Al, Fe, Si all precipitated and filtered out).

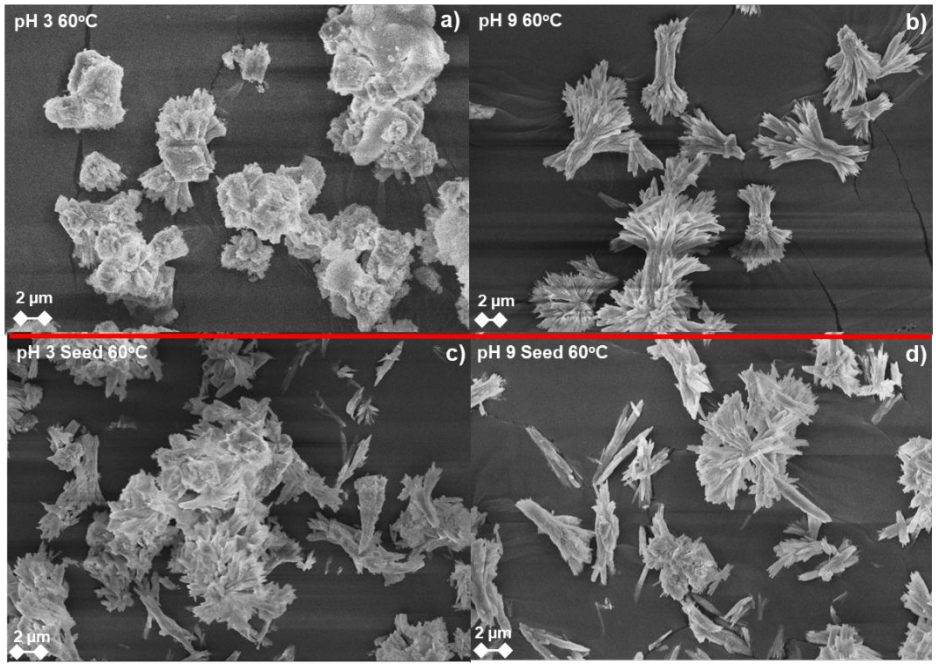

Figure 3.12. SEM micrographs of unseeded PCC production (top row) and seeded PCC production of aragonite (bottom row) using pH 3 and pH 9 leachates at 60°C.

3.7. Reincorporation of aragonite into new cement admixtures and its potential uses

The influence of calcite and aragonite on the hydration kinetics of OPC is shown in **Figure 3.13a**. Aragonite was tested for advantages relative to calcite, a proxy for limestone, which is the most common filler for cement substitution. Replacement of cement by 20 wt.% aragonite accelerated the hydration of cement, as the initial peak was much higher than that of calcite and OPC. This can be attributed to a "filler effect"; the high surface area of aragonite (~8 m^2/g) can provide additional sites for the nucleation of cement hydrated phases, such as calcium silicate hydrate (C-S-H).[68,69] The anhydrous polymorphs of calcite carbonate have been shown to modify the hydration kinetics of cement through this filler effect in additional studies.[26] The replacement of OPC with calcium carbonates, with potential advantageous properties and without any damage to the integrity of the material is of extreme importance in a carbon-constrained world. This allow for multiple aspects of CO_2 savings: firstly, in the capture of CO_2 to synthesize various morphologies aof calcium carbonate; secondly, to replace a portion of OPC with these carbonates to offset emissions associated with cement clinker production.

Rheological measurements of the samples revealed that 20 wt.% aragonite substitution dramatically increased the static yield stress of the samples (**Fig. 3.14b**). This effect was recently studied by Zhao et al. (2023), who observed that the high surface area, needle-like habit, and smaller PSD of aragonite allowed for a high static yield stress due to the formation of 3D network in the suspensions, increasing the chances of physical particle interaction.[27] In addition, a greater structural build-up rate was observed due to the higher extent of acceleration of cement hydration at the early period versus calcite or vaterite. Li et al. (2019) also observed a similar rheological modification of cement pastes when introducing aragonite and calcite whiskers.[70] The increasing cement replacement level by these materials led to an increase in static yield stress. The elevated static yield stress and enhanced structural build-up rate make aragonite a promising rheology modifier, which could be particularly useful in applications such as 3D printing of concrete for advanced manufacturing. The realization of the uses of aragonite as a built environment input and construction material allow for the diversification of CCU activities and give motivation towards the synthesis of the polymorphs of calcium carbonate.

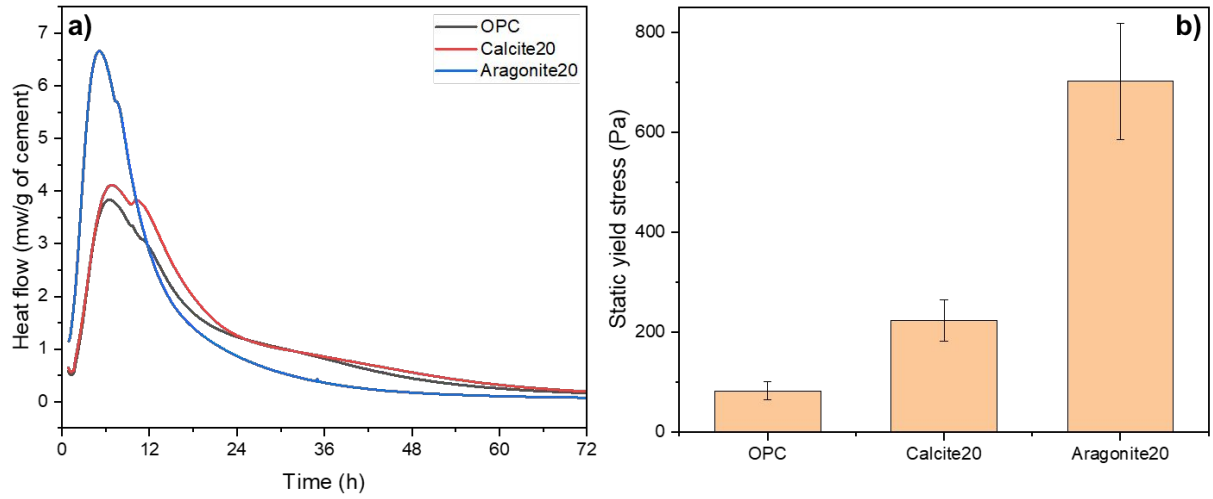

Figure 3.13. (a) Heat flow and for 20%-substituted OPC with calcite and aragonite as measured over 72 and hours, respectively. **(b)** Static yield stress development for 20%-substituted OPC with calcite and aragonite.

3.8. Proposed seeding mechanism for directed synthesis of aragonite for carbon capture and utilization (CCU)

The nuances of the proposed seeding mechanism observed in this study are presented in **Figure 3.14**, which shows both the classical batch method to make aragonite PCC synthetically and an optimized method using seeding combined with semi-continuous crystallization. As the temperature of the reactor increases, the growth rate of aragonite is promoted and the nucleation of the less stable phases at these high temperatures, vaterite and calcite, is suppressed. Previous research has shown that temperatures greater than 60°C are generally necessary for appreciable or near-pure amounts of aragonite to form[6,11,12]; however, this critical temperature is dependent on reactor type, solute concentrations, and hydrodynamics. This temperature could be lower if additives are utilized, such as Mg^{2+}, which has been shown to suppress calcite nucleation, even at ambient temperatures.[45,59] A challenge with utilizing Mg additives is to prevent the secondary and potentially undesired formation of $MgCO_3$, which could co-precipitate with the PCC.

At low solute concentrations, the formation of pure aragonite at elevated temperatures is easily promoted. However, at scale higher solute concentrations could be utilized to improve the per-pass yield, which in turn could increase the supersaturation of undesired phases, such as calcite or vaterite, leading to an impure product. In a more practical and controlled approach, a seed bed of aragonite can be introduced, which can supply proper nucleation sites for ACC to directly convert to aragonite or for vaterite to re-crystallize to aragonite after it dissolves and reprecipitates. As such, crystal seeds can reduce the free energy required to form metastable phases without additives using heterogeneous surfaces, and serve as templates to direct aragonite growth in the crystallizer.[39] Using this seeded semi-continous system, pure aragonite can be formed at lower temperatures (40 °C) and even ambient conditions (25 °C) under the proper calcium injection conditions. At scale, semi-continuous seeded production of aragonite would be desired due to ease of operation and process intensification, which allows for a continuous draw of product. Additionally, seed can be continually circulated through the reactor to replenish the product which is drawn off. The ability to improve the overall energetic requirements for aragonite production at scale is also advantageous to minimize risk and reduce consumption if waste heat is not available.

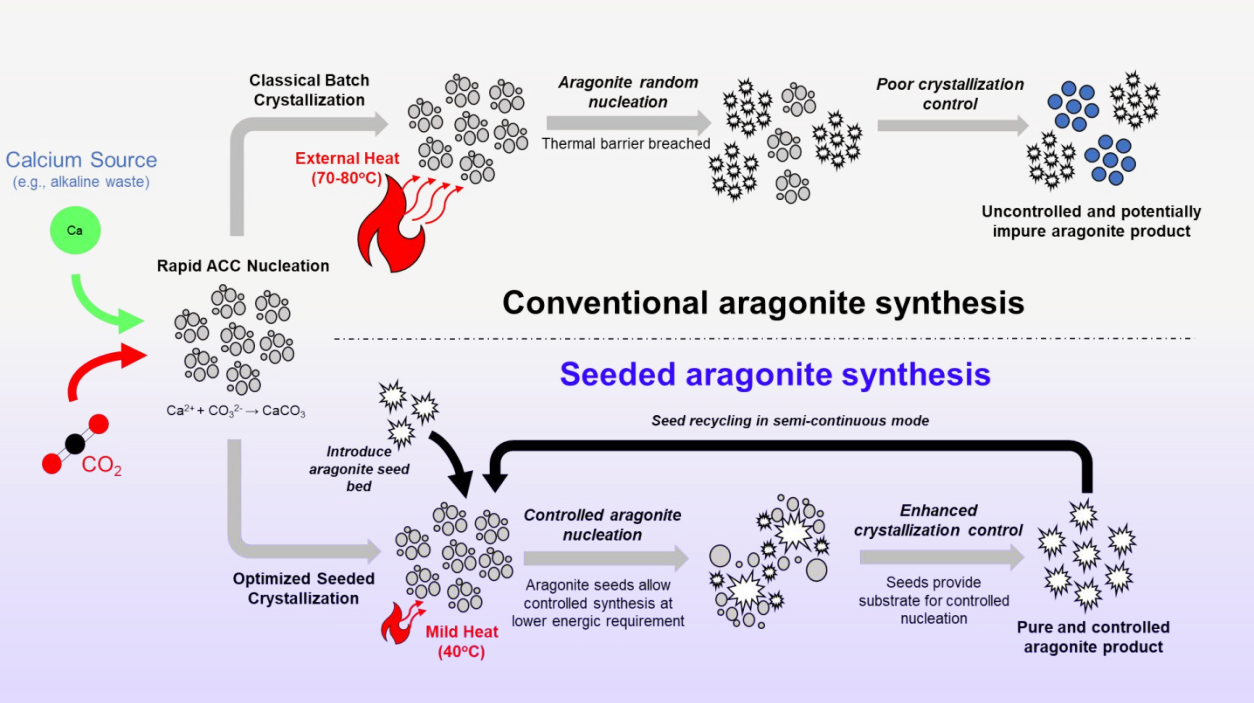

Figure 3.14. Schematic showing the advantages of a directed synthesis of aragonite using seeded crystallization methods compared to conventional methods of synthetic aragonite production with poor control.

4. Conclusions

In this study, novel directed crystallization methods were applied to aragonite synthesis in an effort to motivate its production as a potential commodity in the carbon economy of the future. Anhydrous PCC crystal seeds were synthesized and characterized. Batch and semi-continuous crystallizers were used in both seeded and un-seeded operation to evaluate the production of PCC from calcium derived from model salts (i.e., $CaCl_2$) and also as leached from waste hydrated cement paste. The principle variables tested were temperature, seed loading, Ca solvent injection rate, crystallizer mixing method, and the effect of impurities on seeded process. The produced crystals were analyzed via comprehensive characterization techniques, including SEM, PSA, PXRD, BET, FTIR, and EDS. Based on the data presented in this study, the following conclusions can be drawn:

- Gaseous CO_2 can be loaded into aqueous carbonate salts with a CO_2 capture efficiency of >85%. In this case, KOH was used to produce K_2CO_3 as a salt to facilitate the production of PCC from calcium. Using highly soluble aqueous salts could reduce mass-transfer limitations during crystallizations afforded by CO_2 solubility issues. Using K_2CO_3 as a carbon-carrier allows for enhanced crystallization control for the synthesis of PCC.
- 20% aragonite replacement in cement increases the hydration rate of cement but results in a lower overall cumulative hydration acceleration due to OPC displacement. Aragonite replacement in OPC yields greater dynamic/static stress attributed to a viscosity-effect due to needle-like particles.
- Semi-continuous crystallization can form aragonite at lower temperatures than batch systems due to enhanced mixing and suppression of calcite nucleation imparted by the re-circulation route. This preferentially allows for the nucleation of metastable aragonite versus calcite at lower temperatures.
- Seeded semi-continuous aragonite crystallization can increase the phase purity of the same to close to 78-82% at room temperature, demonstrating the energetic advantages towards using seeding in the production of aragonite.

- Flow analysis revealed the tank conditions as being turbulent with the recirculating loop being in laminar flow. Similar mixing times within the bulk tank (0.897 s) and the injection recirculating loop (1.87 s) were established. The similarities in mixing behavior suggest that the hydrodynamic differences could be more responsible for the observed aragonite phase purity enhancement than mixing alone.
- Ca-injection rate has no strong impact on product composition in batch systems, but can greatly increase aragonite formation at low rates in semi-continuous operation, a potential advantage of such systems.
- Removal of PMO from Ca-leachate prior to carbonation significantly improves carbonate purity and allows for better crystallization control to form metastable vaterite and aragonite versus calcite; however, seeding with aragonite boosts its phase purity and yield, even with impurities present.

Author Contributions

J.M.W., A.-H.P., and A.J.M. conceived, planned, and designed this study. J.M.W. executed the majority of the experimental work, analytical analysis, and wrote the manuscript. D.Z. supplied the hydration and rheological data and wrote the subsequent interpretations. N.Z. assisted in data analysis, interpretation, editing, and publishing. A.C. assisted with the semi-continuous crystallization and HCP leaching experiments. S.K. offered interpretation regarding the behavior of carbonate polymorphs in cement systems and assisted with drafting and editing.

Conflicts of Interest

The authors declare that they have no known competing financial interests or personal relationship that could have appeared to influence the work reported herein.

Acknowledgements

This work was supported by the New York State Energy Research & Development Authority (NYSERDA, Albany, New York), Agreement Number: 0000185059 and the Lenfest Center for Sustainable Energy (Columbia University, New York, New York). The authors acknowledge the use of facilities and instrumentation supported by NSF through the Columbia University, Columbia Nano Initiative, and the Materials Research Science and Engineering Center DMR-2011738.

References:

1 S. Chu and A. Majumdar, *Nature*, 2012, **488**, 294–303.
2 B. Smit, A. H. A. Park and G. Gadikota, *Front. Energy Res.*, 2014, **2**, 55.
3 N. Mac Dowell, P. S. Fennell, N. Shah and G. C. Maitland, *Nat. Clim. Chang. 2017 74*, 2017, **7**, 243–249.
4 P. Kelemen, S. M. Benson, H. Pilorgé, P. Psarras and J. Wilcox, *Front. Clim.*, 2019, **1**, 9.
5 V. Romanov, Y. Soong, C. Carney, G. E. Rush, B. Nielsen and W. O'Connor, *ChemBioEng Rev.*, 2015, **2**, 231–256.
6 R. Chang, S. Kim, S. Lee, S. Choi, M. Kim and Y. Park, *Front. Energy Res.*, 2017, **5**, 1–12.
7 G. Gadikota, K. Fricker, S.-H. Jang and A.-H. A. Park, *ACS Symp. Ser.*, 2015, 295–322.
8 G. Gadikota, J. Matter, P. Kelemen, P. V Brady and A. A. Park, *Fuel*, 2020, **277**, 117900.
9 S. Yadav and A. Mehra, , DOI:10.1007/s11356-020-12049-4/Published.
10 G. Rim, N. Roy, D. Zhao, S. Kawashima, P. Stallworth, S. G. Greenbaum and A.-H. A. Park, *Faraday Discuss.*, , DOI:10.1039/d1fd00022e.
11 F. Liendo, M. Arduino, F. A. Deorsola and S. Bensaid, *Powder Technol.*, 2022, **398**, 117050.
12 R. Chang, D. Choi, M. H. Kim and Y. Park, *ACS Sustain. Chem. Eng.*, 2017, **5**, 1659–1667.
13 R. A. Boulos, F. Zhang, E. S. Tjandra, A. D. Martin, D. Spagnoli and C. L. Raston, *Sci. Reports 2014 41*, 2014, **4**, 1–6.
14 J. Y. Gal, J. C. Bollinger, H. Tolosa and N. Gache, *Talanta*, 1996, **43**, 1497–1509.

15 R. Oyanagi, A. Okamoto, M. Satish-Kumar, M. Minami, Y. Harigane and K. Michibayashi, *Commun. Earth Environ. 2021 21*, 2021, **2**, 1–10.
16 I.-L. Microsc, ; H Zar, L. Saiman, L. Quittell, A. Prince, ; L Imundo, J. Barasch and Q. Al-Awqati, *Science (80-.).*, 1996, **271**, 67–69.
17 N. Conci, S. Vargas and G. Wörheide, *Front. Ecol. Evol.*, 2021, **9**, 623774.
18 D. J. Shearman, J. Twyman and M. Zand Karimi, *Proc. Geol. Assoc.*, 1970, **81**, 561–575.
19 R. Chang, D. Choi, M. H. Kim and Y. Park, *ACS Sustain. Chem. Eng.*, 2017, **5**, 1659–1667.
20 W. Sun, S. Jayaraman, W. Chen, K. A. Persson and G. Ceder, *Proc. Natl. Acad. Sci. U. S. A.*, 2015, **112**, 3199–3204.
21 P. N. Gavryushkin, A. B. Belonoshko, N. Sagatov, D. Sagatova, E. Zhitova, M. G. Krzhizhanovskaya, A. Rečnik, E. V. Alexandrov, I. V. Medrish, Z. I. Popov and K. D. Litasov, *Cryst. Growth Des.*, 2021, **21**, 65–74.
22 S. J. Köhler, P. Cubillas, J. D. Rodríguez-Blanco, C. Bauer and M. Prieto, *Environ. Sci. Technol.*, 2007, **41**, 112–118.
23 T. Thenepalli, A. Y. Jun, C. Han, C. Ramakrishna and J. W. Ahn, *Korean J. Chem. Eng.*, 2015, **32**, 1009–1022.
24 Z. Hu, M. Shao, H. Li, Q. Cai, C. Zhong, Z. Xianming and Y. Deng, *Adv. Compos. Mater.*, 2012, **18**, 315–326.
25 P. Shen, J. Lu, Y. Zhang, Y. Jiang, S. Zhang and C. S. Poon, *Cem. Concr. Res.*, 2022, **159**, 106891.
26 D. Zhao, J. M. Williams, Z. Li, A.-H. A. Park, A. Radlińska, P. Hou and S. Kawashima, *Cem. Concr. Res.*, 2023, **173**, 107270.
27 D. Zhao, J. M. Williams, A. H. A. Park and S. Kawashima, *Cem. Concr. Res.*, 2023, **172**, 107214.
28 O. A. Jimoh, K. S. Ariffin, H. Bin Hussin and A. E. Temitope, *Carbonates Evaporites 2017 332*, 2017, **33**, 331–346.
29 N. Zhang and A. Moment, *ACS Sustain. Chem. Eng.*, , DOI:10.1021/acssuschemeng.2c04241.
30 J. Chen and L. Xiang, *Powder Technol.*, 2009, **189**, 64–69.
31 F. Liendo, M. Arduino, F. A. Deorsola and S. Bensaid, *J. Cryst. Growth*, 2022, **578**, 126406.
32 O. Cherkas, T. Beuvier, F. Zontone, Y. Chushkin, L. Demoulin, A. Rousseau and A. Gibaud, *Adv. Powder Technol.*, 2018, **29**, 2872–2880.
33 D. Konopacka-łyskawa, N. Czaplicka, M. Łapiński, B. Kościelska and R. Bray, *Materials (Basel).*, 2020, **13**, 1–14.
34 J. M. Walker, B. Marzec and F. Nudelman, *Angew. Chemie Int. Ed.*, 2017, **56**, 11740–11743.
35 Y. Xu and N. A. J. M. Sommerdijk, *Proc. Natl. Acad. Sci. U. S. A.*, 2018, **115**, 8469.
36 M. Zeng, Y. Y. Kim, C. Anduix-Canto, C. Frontera, D. Laundy, N. Kapur, H. K. Christenson and F. C. Meldrum, *Proc. Natl. Acad. Sci. U. S. A.*, 2018, **115**, 7670–7675.
37 N. Zhang, R. M. Santos, S. M. Smith and L. Šiller, *Chem. Eng. J.*, 2019, **377**, 120479.
38 A. S. Myerson and R. Ginde, in *Handbook of Industrial Crystallization*, 2002, pp. 33–65.
39 Y. He, Z. Gao, T. Zhang, J. Sun, Y. Ma, N. Tian and J. Gong, *Org. Process Res. Dev.*, 2020, **24**, 1839–1849.
40 E. J. Swanson, K. J. Fricker, M. Sun and A. H. A. Park, *Phys. Chem. Chem. Phys.*, 2014, **16**, 23440–23450.
41 R. A. Berner, *Geochim. Cosmochim. Acta*, 1975, **39**, 489–504.
42 W. Omara, H. Al-Zoubib and J. Ulrichc, *Desalin. water Treat.* , 2009, **3**, 236–240.
43 H. El Fil, A. S. Manzola and M. Ben Amor, *Appl. Geochemistry*, 2003, **18**, 1137–1148.
44 H. Imai, T. Terada, T. Miura and S. Yamabi, *J. Cryst. Growth*, 2002, **244**, 200–205.
45 W. K. Park, J. W. Ahn, S. J. Ko and C. Han, *Mater. Sci. Forum*, 2007, **544–545**, 693–696.
46 S. Tadier, S. Rokidi, C. Rey, C. Combes and P. G. Koutsoukos, *J. Cryst. Growth*, 2017, **458**, 44–52.
47 N. S. Tavare, in *Industrial Crystallization*, Springer, Boston, MA, 1995, pp. 415–463.
48 T. Tari, P. Szabó-Révész and Z. Aigner, *Cryst. 2019, Vol. 9, Page 295*, 2019, **9**, 295.

49 P. H. Karpiński and J. Bałdyga, in *Handbook of Industrial Crystallization*, 2019, pp. 216–265.
50 A. A.-H. Mourad, A. F. Mohammad, A. H. Al-Marzouqi, M. Altarawneh, M. H. Al-Marzouqi and H. El-Naas, *Int. J. Greenh. Gas Control*, 2022, **120**, 103768.
51 S. Kim, J. Jeon and M. J. Kim, *J. Environ. Chem. Eng.*, 2022, **10**, 107296.
52 T. F. Kazmierczak, M. B. Tomson and G. H. Nancollas, *J. Phys. Chem.*, 1982, **86**, 103–107.
53 N. V. Vagenas, A. Gatsouli and C. G. Kontoyannis, *Talanta*, 2003, **59**, 831–836.
54 F. B. Reig, J. V. G. Adelantado and M. C. M. Moya Moreno, *Talanta*, 2002, **58**, 811–821.
55 E. L. Paul, V. A. Atiemo-Obeng and S. M. Kresta, *Handbook of industrial mixing : science and practice*, Wiley-Interscience, 2004.
56 M. Ghiasi, M. Abdollahy, M. R. Khalesi and E. Ghiasi, *CrystEngComm*, 2020, **22**, 1970–1984.
57 M. Ukrainczyk, J. Kontrec, V. Babić-Ivančić, L. Brečević and D. Kralj, *Powder Technol.*, 2007, **171**, 192–199.
58 M. G. Lioliou, C. A. Paraskeva, P. G. Koutsoukos and A. C. Payatakes, *J. Colloid Interface Sci.*, 2007, **308**, 421–428.
59 W. K. Park, S. J. Ko, S. W. Lee, K. H. Cho, J. W. Ahn and C. Han, *J. Cryst. Growth*, 2008, **310**, 2593–2601.
60 J. H. Burns and M. A. Bredig, *J. Chem. Phys.*, 1956, **25**, 1281.
61 R. M. Santos, P. Ceulemans and T. Van Gerven, *Chem. Eng. Res. Des.*, 2012, **90**, 715–725.
62 C. Ramakrishna, T. Thenepalli, J.-H. Huh, J. W. Ahn, C. Ramakrishna, T. Thenepalli, J.-H. Huh and J. W. Ahn, *J. Korean Ceram. Soc.*, 2016, **53**, 222–226.
63 J. Jiang, S. F. Chen, L. Liu, H. Bin Yao, Y. H. Qiu, M. R. Gao and S. H. Yu, *Chem. Commun.*, 2009, **0**, 5853–5855.
64 J. Chen and L. Xiang, *Powder Technol.*, 2009, **189**, 64–69.
65 M. Kellermeier, E. Melero-García, F. Glaab, R. Klein, M. Drechsler, R. Rachel, J. M. García-Ruiz and W. Kunz, *J. Am. Chem. Soc.*, 2010, **132**, 17859–17866.
66 S. Hong, S. Moon, G. Sim and Y. Park, *J. CO2 Util.*, 2023, **69**, 102418.
67 G. Sim, S. Hong, S. Moon, S. Noh, J. Cho, P. T. Triwigati, A. H. A. Park and Y. Park, *J. Environ. Chem. Eng.*, 2022, **10**, 107327.
68 B. Lothenbach, K. Scrivener and R. D. Hooton, *Cem. Concr. Res.*, 2011, **41**, 1244–1256.
69 A. Kumar, T. Oey, G. Falzone, J. Huang, M. Bauchy, M. Balonis, N. Neithalath, J. Bullard and G. Sant, *J. Am. Ceram. Soc.*, 2017, **100**, 3316–3328.
70 L. Li, M. Cao and H. Yin, *Cem. Concr. Compos.*, 2019, **104**, 103350.